J Arid Land (2014) 6(6): 704–716
doi: 10.1007/s40333-014-0071-z
jal.xjegi.com; www.springer.com/40333

Land surface temperature retrieval for arid regions based on Landsat-8 TIRS data: a case study in Shihezi, Northwest China

Lei YANG[1], YunGang CAO[1], XiaoHua ZHU[2], ShengHe ZENG[3], GuoJiang YANG[3], JiangYong HE[3], XiuChun YANG[4,5*]

[1] Department of Remote Sensing and Geographic Information Engineering, Faculty of Geosciences and Environmental Engineering, Southwest Jiaotong University, Chengdu 611756, China;
[2] Institute of Geographic Sciences and Natural Resources Research, Chinese Academy of Sciences, Beijing 100101, China;
[3] Institute of Farmland Water Conservancy and Soil-fertilizer, Xinjiang Academy of Agricultural and Reclamation Science, Shihezi 832000, China;
[4] Institute of Agricultural Resources and Regional Planning, Chinese Academy of Agricultural Sciences, Beijing 100081, China;
[5] College of Environment and Planning, Shangqiu Normal University, Shangqiu 476000, China

Abstract: Scientific interest in geophysical information about land surface temperature (LST) is ever increasing, as such information provides a base for a large number of applications, including environmental and agricultural monitoring. Therefore, the research of LST retrieval has become a hot topic. Recent availability of Landsat-8 satellite imagery provides a new data source for LST retrieval. Hence, exploring an adaptive method with reliable accuracy seems to be essential. In this study, basing on features of Landsat-8 TIRS thermal infrared channels, we re-calculated parameters in the atmospheric transmittance empirical models of the existing split-window algorithm, and estimated the ground emissivity with the help of the land cover classification map of the study area. Furthermore, a split-window algorithm was rebuilt by virtual of the estimation model of the updated atmospheric transmittance and the ground emissivity, and then a remote sensing retrieval for the LST of Shihezi city in Xinjiang Uygur autonomous region of Northwest China was conducted on the basis of this modified algorithm. Finally, precision validation of the new model was implemented by using the MODIS LST products. The results showed that the LST retrieval from Landsat-8 TIRS data based on our algorithm has a higher credibility, and the retrieved LST is more consistent with the MODIS LST products. This indicated that the modified algorithm is suitable for retrieving LST with competitive accuracy. With higher resolutions, Landsat-8 TIRS data may provide more accurate observation for LST retrieval.

Keywords: thermal infrared remote sensing; land surface temperature retrieval; split-window algorithm; Landsat-8 TIRS

Citation: Lei YANG, YunGang CAO, XiaoHua ZHU, ShengHe ZENG, GuoJiang YANG, JiangYong HE, XiuChun YANG. 2014. Land surface temperature retrieval for arid regions based on Landsat-8 TIRS data: a case study in Shihezi, Northwest China. Journal of Arid Land, 6(6): 704–716. doi: 10.1007/s40333-014-0071-z

Earth surface temperature, including water surface temperature and land surface temperature (LST), refers to the temperature of the critical layer by which the earth surface interacts with the atmosphere. Earth surface temperature is an important parameter reflecting earth surface environment, and is widely used in several research fields such as climate change, agricultural drought monitoring and urban heat island effect (Friedel, 2012; Son et al., 2012; Maimaitiyiming et al., 2014).

The traditional method to obtain LST is a measurement at fixed observation time and location by a

*Corresponding author: XiuChun YANG (E-mail: yangxiuchun@caas.cn)
Received 2014-01-09; revised 2014-03-03; accepted 2014-04-14
© Xinjiang Institute of Ecology and Geography, Chinese Academy of Sciences, Science Press and Springer-Verlag Berlin Heidelberg 2014

thermometer. Due to the variable changes of LST, the method of discrete point measurement cannot obtain large-scale and continuous LST information. However, the development of satellite thermal infrared remote sensing technology makes it possible to get the LST distribution over large regions with a regular revisit capability (Peng et al., 2014). Since the 1980s, numerous studies have been conducted to explore the feasibility and accuracy of image analysis applications for LST retrieval (Vinnikov et al., 2011; Li et al., 2013). A variety of algorithms, such as mono-window algorithm, split-window algorithm and multi-channel algorithm (Qin et al., 2001a; Katsiabani et al., 2009; Zhou et al., 2010), have been proposed to obtain LST on account of the characteristics of different data and actual application situations.

Currently, thermal infrared satellite sensors that can be used for retrieving LST mainly include NOAA-AVHRR, EOS-MODIS, Advanced Spaceborne Thermal Emission and Reflection Radiometer (ASTER), Landsat TM/ETM+, HJ-1B IRS and CBERS-02 IRMSS (Wan, 2008; Jiménez-Muñoz et al., 2010; Li et al., 2010). Among these, mono-window algorithm is suitable for Landsat TM/ETM+ and HJ-1B IRS, which contain only one thermal infrared channel; split-window algorithm is suitable for NOAA-AVHRR and EOS-MODIS, which include two thermal infrared channels; and multi-channel algorithm is suitable for EOS-MODIS and ASTER, which can provide sufficient observational information from multiple channels.

Landsat series satellites of USA played an incomparable role in the monitoring of ecological environment changes at the global scale. TM contains a thermal infrared band with a spatial resolution of 120 m. While the ETM+ is obtained by one thermal infrared band appearing in both channels, with the data in channel one fixed in high gain (6H) and the data in channel two fixed in low gain (6L), and the spatial resolution is 60 m. According to these characteristics, Qin et al. (2001b) proposed a mono-window algorithm, while Jiménez-Muñoz and Sobrino (2003) put forward a generalized single-channel algorithm. Both of their algorithms do not rely on the data of real-time vertical atmospheric profile and radiation transfer model, and can achieve high accuracies. In addition, the relative higher spatial resolutions of TM/ETM+ thermal infrared data enable the data be widely concerned in the applications that require accurate regional analysis of relevant surface temperature (Srivastava et al., 2009; Ma et al., 2010).

Landsat-8 was successfully launched by United States Geological Survey (USGS) and National Aeronautics and Space Administration (NASA) on 11 February 2013. The Operational Land Imager (OLI) carried by Landsat-8 has nine spectral bands with a spatial resolution of 30 m, including one 15-m panchromatic band which is mainly used to obtain remote sensing images in the visible, near infrared and shortwave infrared spectral ranges. In particular, the Thermal Infrared Sensor (TIRS) carried by Landsat-8 sets up two thermal infrared spectral bands (10.60–11.19 and 11.50–12.51 μm, respectively) with a spatial resolution of 100 m by dividing the thermal infrared wave band based on the formal Landsat-7 (Irons et al., 2012). Therefore, split-window algorithm can be used to eliminate atmospheric effects, and then obtain LST retrieval results with a relatively higher accuracy.

In this study, basing on the characteristics of Landsat-8 TIRS data, we made relevant revision to the empirical relationship of Qin's algorithm (Qin et al., 2001c) applied to NOAA-AVHRR thermal infrared data, and then applied this modified algorithm to retrieve the LST of Shihezi city and gave a quantitative evaluation for this algorithm.

1 Study area and data source

1.1 Study area

Shihezi city is located in the northern part of Xinjiang Uygur autonomous region and on the northern slope of central Tianshan Mountains (84°45′–86°40′E, 43°20′–45°20′N; 300–500 m asl; Fig. 1). From south to north, its terrain forms are Tianshan Mountains area, mountain piedmont hilly area, piedmont plain and alluvial plain. The region is characterized by a temperate continental climate. The annual average temperature is 6.5°C–7.2°C, with the maximum in July and the minimum in January. The average annual precipitation 125.0–207.7 mm, while the average annual evapotran-

spiration is 1,000–1,500 mm. As Shihezi region is a typical arid irrigated agricultural area, the use of remote sensing techniques to conduct researches on LST retrieval at a regional scale has a positive significance for the ecological construction and sustainable agricultural development in this region.

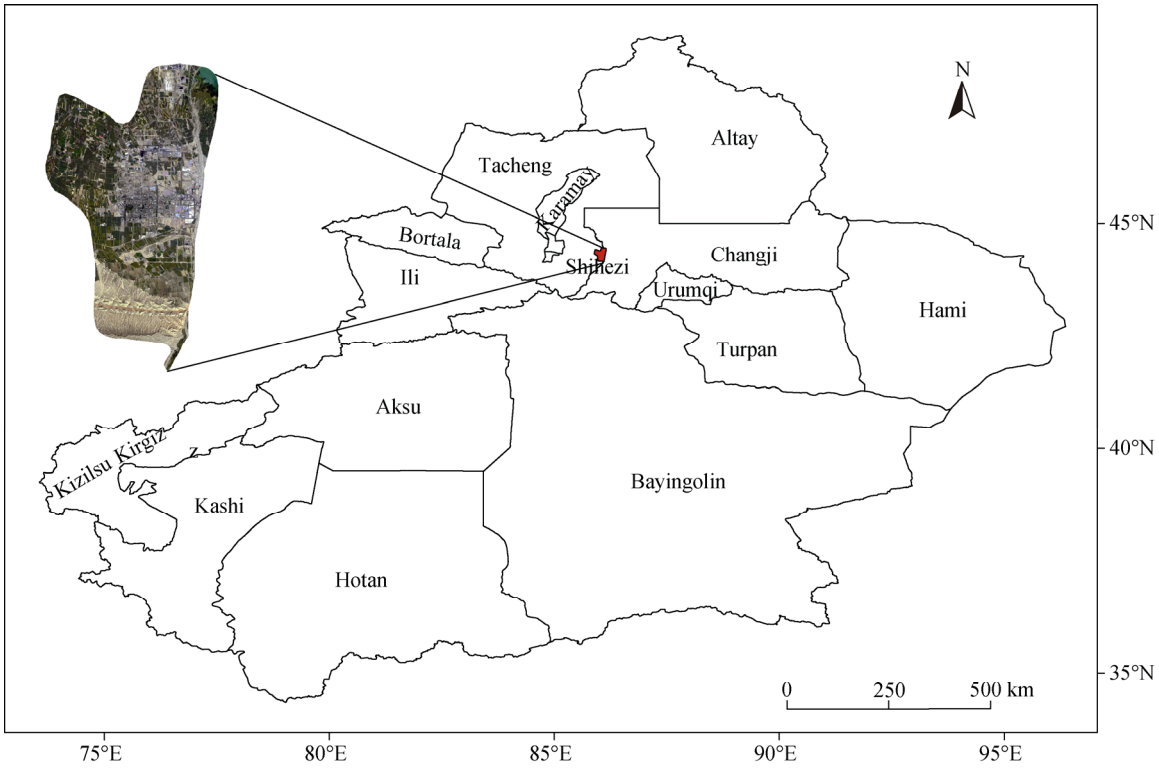

Fig. 1 Location of the study area

1.2 Data source and preprocessing

In this study, Landsat-8 L1T data provided by USGS were acquired at 13:04 on 4 September 2013, with a track number of 144/29 and 1% image mean cloudiness. MODIS LST/emissivity products (MOD11A1) at the same day were provided by NASA, with a track number of h24v04 and a spatial resolution of 1 km. Moreover, automatic weather station (AWS) observational data such as surface vapor pressure surrounding the study area were collected from the website of the local bureau of meteorology according to the satellite transit time.

For data preprocessing, three procedures were implemented. Firstly, radiometric calibration and atmospheric correction were made to the OLI imagery by referring to the header file information. In this procedure, Digital Number (DN) values recorded by the sensor were converted into apparent reflectance and satellite brightness temperature for OLI and TIRS data, respectively. Then TIRS data were resampled in a 30-m resolution. Secondly, the format conversion and projection transformation (from Sinusoidal projection to UTM/WGS1984) of MODIS LST products was performed via the MODIS Reprojection Tool (MRT). The original DN values were transformed into LST, too. Finally, the data required for the LST retrieval and its validation were collected by clipping the above images according to the vector boundaries of the study area.

2 LST retrieval method based on Landsat-8 TIRS data

2.1 Transfer equation of the land surface thermal radiation

The thermal radiation received by the sensor mainly includes three parts: surface thermal radiation after

atmospheric attenuation, upwelling atmospheric thermal radiation and downwelling atmospheric thermal radiation with atmospheric attenuation after being reflected by the surface and eventually received by the remote sensor (Qin et al., 2001a). Therefore, transfer equation of the land surface thermal radiation can be expressed as Eq. 1.

$$B_i(T_i) = \tau_i(\theta)[\varepsilon_i B_i(T_s) + (1-\varepsilon_i)I_i\downarrow] + I_i\uparrow. \quad (1)$$

Where, $B_i(T_i)$ is the radiation intensity received by the sensor; i is the sensor channel number; T_i is the brightness temperature; $\tau_i(\theta)$ is the atmospheric transmittance in channel i at a viewing angle θ; ε_i is the ground emissivity; T_s is the LST; $B_i(T_s)$ is the ground radiation intensity when the surface temperature is T_s; and $I_i\uparrow$ and $I_i\downarrow$ represent upwelling and downwelling atmospheric radiation intensity, respectively.

Qin et al. (2001a) found that the replacement of downwelling atmospheric radiation with upwelling atmospheric radiation would have an insignificant effect on the estimate of T_s. Thus, the above equation can be simplified as Eq. 2.

$$B_i(T_i) = \varepsilon_i\tau_i(\theta)B_i(T_s) + [1-\tau_i(\theta)][1+(1-\varepsilon_i)\tau_i(\theta)]B_i(T_a). \quad (2)$$

Where, T_a is the upwelling effective mean atmospheric temperature, and $B_i(T_a)$ is the atmospheric thermal radiation intensity when upwelling effective mean atmospheric temperature is T_a.

Therefore, LandSat-8 Bands 10 and 11 can be expressed as Eq. 3 and Eq. 4, respectively.

$$B_{10}(T_{10}) = \varepsilon_{10}\tau_{10}(\theta)B_{10}(T_{10}) + [1-\tau_{10}(\theta)][1+(1-\varepsilon_{10})\tau_{10}(\theta)]B_{10}(T_a), \quad (3)$$

$$B_{11}(T_{11}) = \varepsilon_{11}\tau_{11}(\theta)B_{11}(T_{11}) + [1-\tau_{11}(\theta)][1+(1-\varepsilon_{11})\tau_{11}(\theta)]B_{11}(T_a). \quad (4)$$

2.2 Split-window algorithm

Split-window algorithm, the most mature LST retrieval method by far, was first proposed by McMillin (1975) for estimating sea surface temperature on the basis of AVHRR thermal infrared data. Afterwards, it was applied to retrieve LST by Price et al. (1984). Its basic principle is that the difference between the brightness temperatures in two channels will yield information about the atmospheric attenuation, as the two adjacent thermal infrared spectral windows have different absorption characteristics. Over the past three decades, scholars all over the world have proposed more than 10 kinds of split-window algorithms. Through experimental comparison, Qin et al. (2001c) found that Qin's algorithm was better in terms of calculation accuracy. Due to the approximate characteristics and spectral response curve of Landsat-8 TIRS thermal infrared channels and AVHRR channels 4 and 5, we made some improvements on Qin's algorithm in this study in order to adapt Landsat-8 TIRS data for LST retrieval.

Qin's algorithm is a typical two-factor model which can retrieve LST by using just two factors: ground emissivity and atmospheric transmittance. Its basic form is as Eq. 5.

$$T_s = A_0 + A_1T_{10} - A_2T_{11}. \quad (5)$$

Where A_0, A_1 and A_2 are parameters defined as follows:

$$A_0 = [a_{10}D_{11}(1-C_{10}-D_{10}) - a_{11}D_{10}(1-C_{11}-D_{11})]/(D_{11}C_{10}-D_{10}C_{11}), \quad (6)$$

$$A_1 = 1+[D_{10}+b_{10}D_{11}(1-C_{10}-D_{10})]/(D_{11}C_{10}-D_{10}C_{11}), \quad (7)$$

$$A_2 = D_{10}[1+b_{11}(1-C_{11}-D_{11})]/(D_{11}C_{10}-D_{10}C_{11}), \quad (8)$$

$$C_i = \varepsilon\tau_i(\theta), \quad (9)$$

$$D_i = [1-\tau_i(\theta)][1+(1-\varepsilon)\tau_i(\theta)]. \quad (10)$$

Constants of a_{10}, b_{10}, a_{11} and b_{11} can be obtained from linear expansion of the Planck's radiation equation (Qin et al., 2001a).

2.3 Linear expansion of the Planck's radiation equation

In order to solve the correlation between radiation intensity and brightness temperature in TIRS thermal infrared channels, we explored linear expansion of the Planck's radiation equation. Using the first two approximation of Taylor expansion to express non-linear function Planck's equation, we can achieve higher expansion accuracy and obtain Eq. 11.

$$B_i(T_j) = B_i(T) + \frac{(T_j-T)\partial B_i(T)}{\partial T} = (L_i + T_j - T)\partial B_i(T)/\partial T. \quad (11)$$

Where, $B_i(T_j)$ and $B_i(T)$ represent radiation intensity at

temperatures T_j and T, respectively; when i=10 or 11 and j=10 or 11, T_j represents brightness temperature of Band 10 or 11; if $j=s$, T_j represents LST to be solved; if $j=a$, T_j represents upwelling mean atmospheric temperature; T is brightness temperature; L_i is a temperature-related intermediate variable in Kelvin, which is expressed as follows:

$$L_i = B_i(T_\lambda) / \left[\partial B_i(\mathrm{T}) / \partial T\right]. \quad (12)$$

Planck Formula:

$$B_\lambda(T_\lambda) = \frac{C_1}{\lambda^5\left[e^{C_2/(\lambda T_\lambda)} - 1\right]}. \quad (13)$$

By Eqs. 12 and 13, we can get the equation of L_i:

$$L_i = B_i(T_\lambda) / \left[\partial B_i(T_\lambda) / \partial T\right] = \frac{T^2\lambda}{C_2}(1 - e^{-C_2/\lambda T}). \quad (14)$$

Where, C_1 and C_2 are radiation constants with the values of 3.7415×10^{-16} w·m^2 and 1.4387685×10^4 μm·K, respectively, and λ_i is effective center wavelength of Band i. Since the wavelength intervals of LandSat-8 Bands 10 and 11 are 10.60–11.19 and 11.50–12.51 μm, respectively, effective center wavelengths λ_{10}= 10.9 μm and λ_{11}=12.0 μm are assigned (Irons et al., 2012).

For the relationship between the intermediate parameter L_i introduced in the expansion process and brightness temperature, Gao and Qin (2007) found that linear model $L_i=a_i+b_iT_i$ has a higher accuracy and stability. So linear model $L_i=a_i+b_iT_i$ was used in this study for fitting parameters when T_{10} and T_{11} are within the temperature range of 0°C–70°C (Fig. 2). From Fig. 2, we can get a_{10}= –66.338, b_{10}=0.4463, a_{11}= –70.898 and b_{11}=0.4827.

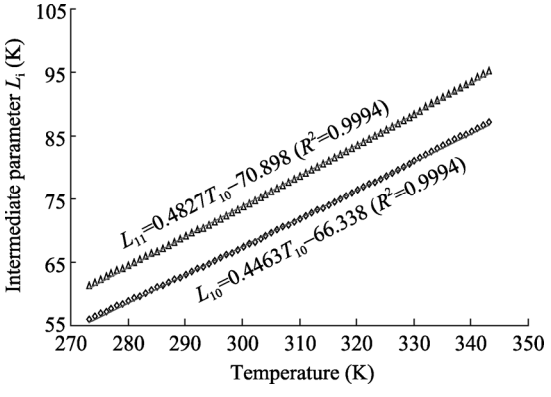

Fig. 2 Relationship of intermediate parameter L_i with temperature

2.4 Ground emissivity

Ground emissivity is a key parameter in LST retrieval model. It uses thermal infrared remote sensing techniques, which mainly depends on the surface material structure and wavelength range of the remote sensor. Emissivity is a measure of the ability of a surface to emit energy by radiation which has a great influence on LST retrieval. Currently, the visible and near- infrared spectra are often used for estimating ground emissivity, such as Van de Griend's empirical formula (Van de Griend and Owe, 1993) and separation method of mixed pixels (Becker and Li, 1995). Each Landsat-8 OLI imagery pixel region (30 m×30 m) could contain two or more land cover types and there is a surface inhomogeneity exists at the pixel scale. So, we used separation method of mixed pixels to estimate the ground emissivity.

As emissivity of different land cover types varies significantly, we used the Gram-Schmidt fusion method of higher image fidelity in this study to make fusion of the Landsat-8 panchromatic band (15 m) with multi-spectral images (30 m), so as to improve the reliability and accuracy of visual interpretation in classification. The fused images could provide increased interpretation capabilities since it enhances the details of spatial features (Fig. 3a). Then supervised classification was performed to divide the study area into water body, town (road, industrial and mining district, city and rural residential area), bare land, grassland and arable land. Lastly, they were reclassified into three categories, namely water body, town and natural surface (including bare land, grassland and arable land).

On the basis previous studies (Sobrino et al., 2001; Stathopoulou et al., 2007), the emissivity of town, vegetation and bare land in pure pixels were assigned as 0.970, 0.986 and 0.972, respectively. As water body pixels are easy to be distinguished and relatively unitary, its emissivity was directly assigned as 0.995. Town pixels can be regarded as the mixture of towns and vegetation. Similarly, natural surface pixels can be regarded as the mixture of vegetation and bare land. Zheng et al. (2010) put forward a set of formulae to estimate the emissivity of town and natural surface, which can be expressed as Eq. 15 and Eq. 16, respectively.

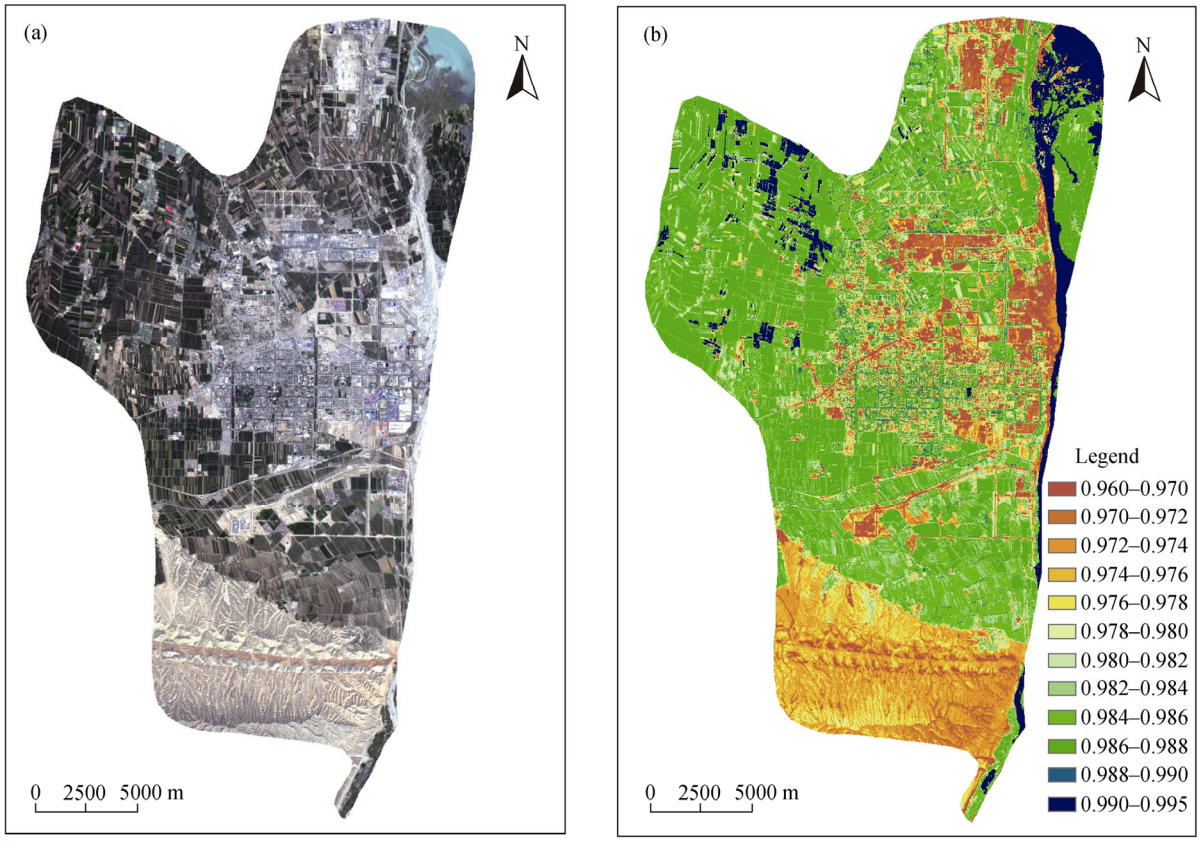

Fig. 3 Gram-Schmidt fusion image (a) and the distribution of ground emissivity (b) for the study area

$$\varepsilon_t = 0.9608420 + 0.0860322 f_c - 0.0671580 f_c^2, \quad (15)$$

$$\varepsilon_n = 0.9643744 + 0.0614704 f_c - 0.0461286 f_c^2. \quad (16)$$

Where f_c represents vegetation cover, which can be calculated by Eq. 17.

$$f_c = (NDVI - NDVI_{\text{soil}}) / (NDVI_{\text{veg}} - NDVI_{\text{soil}}). \quad (17)$$

In Eq. 17, *NDVI* represents normalized differential vegetation index, $NDVI_{\text{veg}}$ is *NDVI* value of pure vegetation area, and $NDVI_{\text{soil}}$ is bare soil or non-vegetation covering area. If there are no obvious vegetation or bare soil pixels in the area, then $NDVI_{\text{veg}}$ and $NDVI_{\text{soil}}$ are assigned 0.7 and 0.05, respectively. Therefore, when $NDVI>0.7$, it can be regarded as full vegetation cover, with both ε_t and ε_n being 0.986; when $NDVI<0.05$, it can be regarded as bare soil, with both ε_t and ε_n being 0.970; when $0.05 \leqslant NDVI \leqslant 0.7$, emissivity can be calculated by Eqs. 15 and 16. Based on the above method, the emissivity of each pixel can be calculated by combining *NDVI*, vegetation coverage and classification map (Fig. 3b).

2.5 Atmospheric transmittance

Atmospheric transmittance mainly depends on the dynamic changes in the amount of water vapor (Qin et al., 2001a). Currently, water vapor content of the atmosphere is usually estimated by using atmospheric software, such as MODTRAN, LOWTRAN and 6S, with standard atmospheric models. It also can be quantitatively retrieved by using absorption characteristics difference of water vapor in the visible, near infrared and thermal infrared bands, such as two-band ratio method (Kaufman and Gao, 1992) and three-band ratio method (Jiang et al., 2006), which were proposed according to the band setting characteristics of MODIS. As water vapor absorption difference in related bands of Landsat-8 cannot be directly used to retrieve atmospheric water vapor content, this study used the relation of water vapor content and surface vapor pressure in the Tianshan Mountains (Eq. 18; Yao, 2012) to estimate the water vapor content in Shihezi region.

$$w = 1.6571e. \quad (18)$$

Where, w is water vapor content in mm, and e is surface vapor pressure in hPa.

To obtain the surface vapor pressure data covering the entire study area, we collected the observation data of 12 automatic weather stations in the surrounding areas of Shihezi during the satellite transit time. We also used inverse distance weighting (IDW) interpolation method to convert point observation into grid data, and resampled its spatial resolution to 30 m. Subsequently, the atmospheric water vapor content can be calculated by Eq. 18.

Lastly, MODTRAN 4 was used to simulate the atmospheric transmittance of two thermal infrared channels of Landsat-8 TIRS under the conditions with the mid-latitudes summer mode, temperature of 25°C and water vapor content of 0.4–3.0 g/cm^2 (Table 1). In order to get a better result of the relationship between atmospheric transmittance and water vapor content, we used piecewise linear fitting method to obtain the universal transmittance estimation equations in the water vapor content ranges of 0.4–1.6 and 1.6–3.0 g/cm^2 (Fig. 4). The flow chart of LST retrieval based on Landsat-8 is shown in Fig. 5.

Table 1 Atmospheric transmittance of TIRS Bands 10 and 11 of Landsat-8

Atmospheric water vapor content (g/cm^2)	τ_{10}	τ_{11}
0.4	0.9565	0.9252
0.6	0.9460	0.9088
0.8	0.9350	0.8919
1.0	0.9236	0.8745
1.2	0.9116	0.8566
1.4	0.8991	0.8380
1.6	0.8861	0.8188
1.8	0.8695	0.7956
2.0	0.8529	0.7727
2.2	0.8340	0.7472
2.4	0.8154	0.7223
2.6	0.7967	0.6969
2.8	0.7775	0.6712
3.0	0.7579	0.6453

3 Results and discussion

3.1 Retrieved LST and its analysis

The LST distribution map of Shihezi city was retrieved by using the improved split-window algorithm according to computed results of ground emissivity and atmospheric transmittance (Fig. 6a).

With the lack of synchronized measured LST data during the satellite transit time, absolute accuracy assessment of retrieved LST cannot be obtained. The current widely used MODIS LST products were used in the experiment for the validation and analysis of the retrieved LST. Wan et al. (2004) found that the accuracy of MODIS LST products is within 1 K. The MODIS LST products in Shihezi are shown in Fig. 6b. Comparing Figs. 6a and b, we can see that spatial distribution is overall consistent between MODIS LST products and the retrieved LST based on Landsat-8 TIRS data. The high temperature regions are located in the south of the Tianshan Mountains area, the mountain piedmont hilly area and urban area.

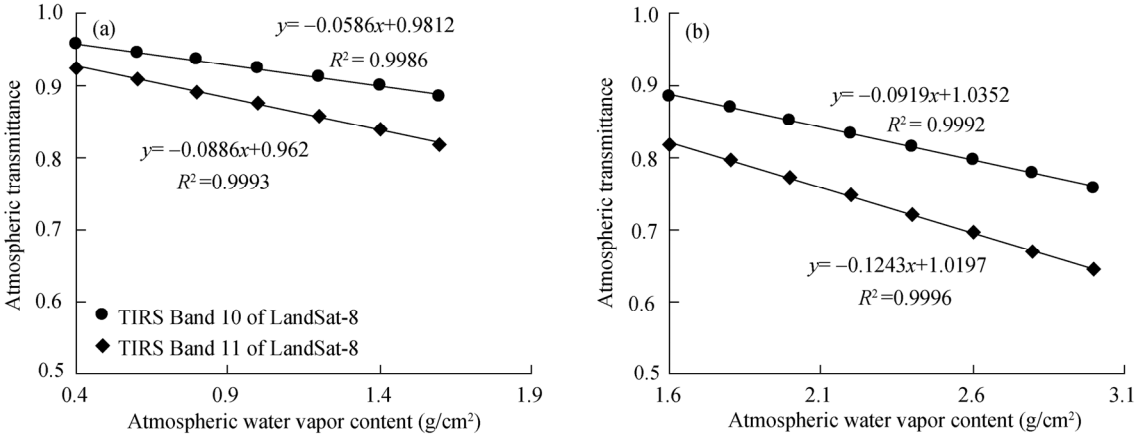

Fig. 4 Fitting relationship between atmospheric transmittance and water vapor content. (a) Water vapor content of 0.4–1.6 g/cm^2; (b) water vapor content of 1.6–3.0 g/cm^2.

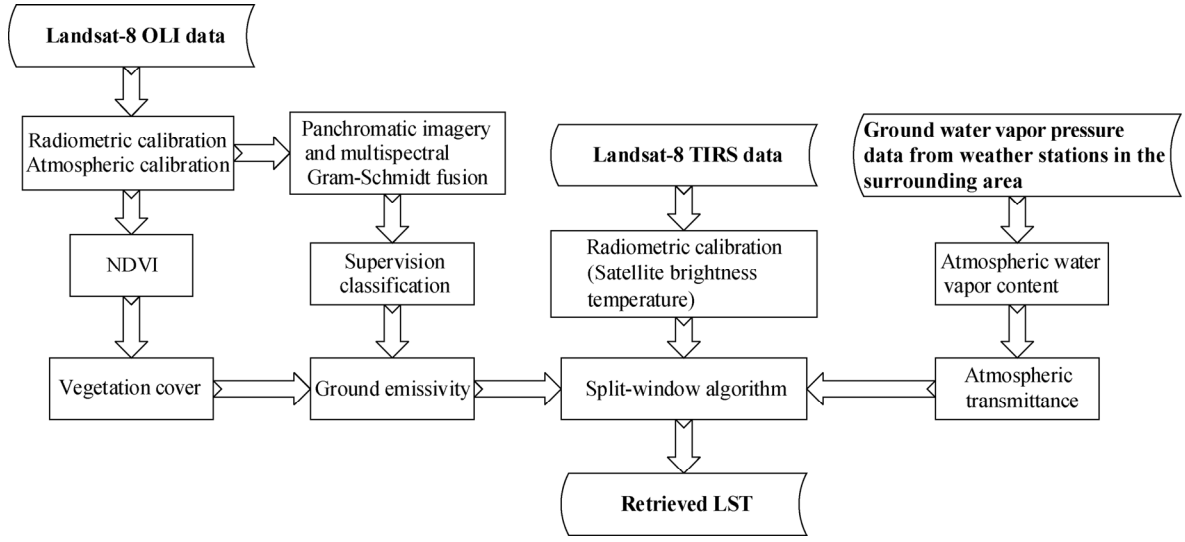

Fig. 5 Flow chart of retrieved land surface temperature (LST)

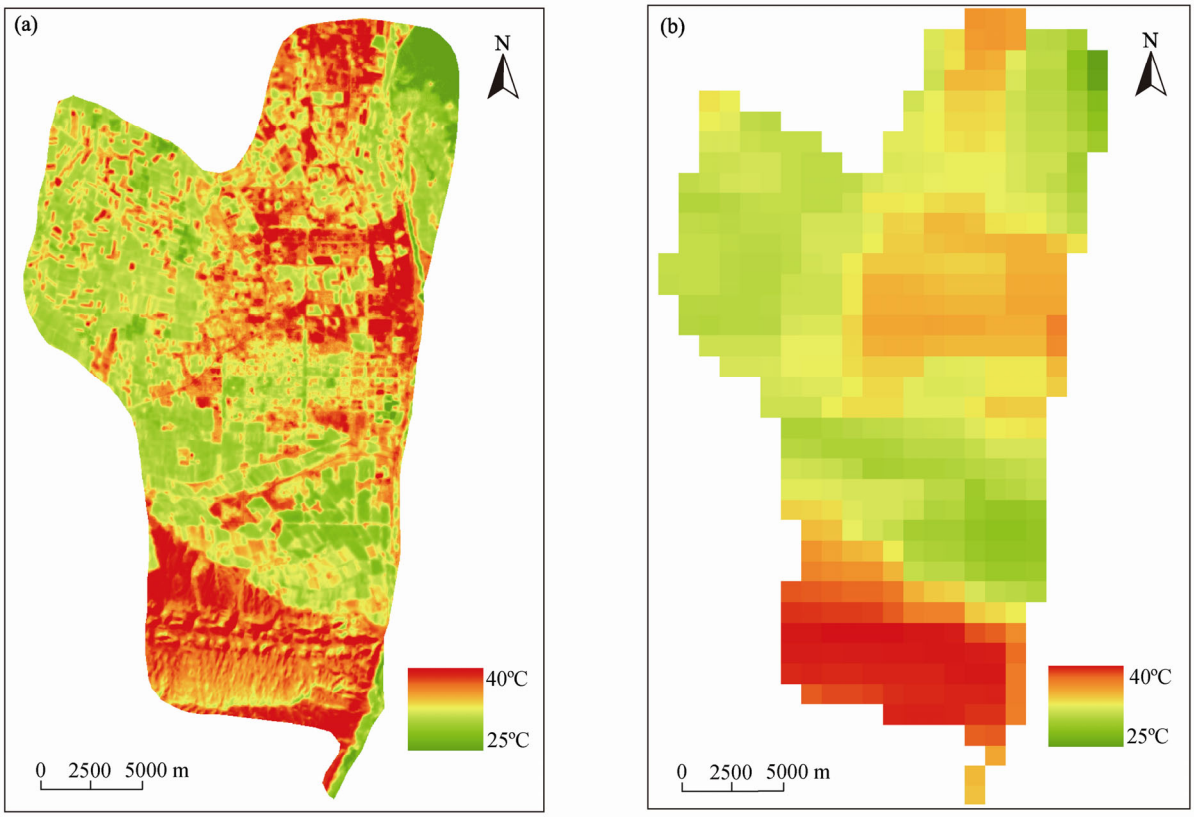

Fig. 6 Retrieved LST based on Landsat-8 TIRS data (a) and MODIS LST products (b) for the study area

The spatial resolution of MODIS LST products is 1 km, while the resolution of retrieved LST in this study is 30 m, thus this two images do not match completely. Therefore, the nearest neighbor interpolation method was used to resample the spatial resolution of retrieved LST based on Landsat-8 TIRS to 1 km at first, then 100 conjugate points between the two images were randomly selected for regression analysis (Fig. 7a). Since MODIS LST products do not include water body, a certain number of conjugate points in

both natural surface and urban area were selected for regression analysis, and their scatter diagrams were drawn respectively (Figs. 7b and c).

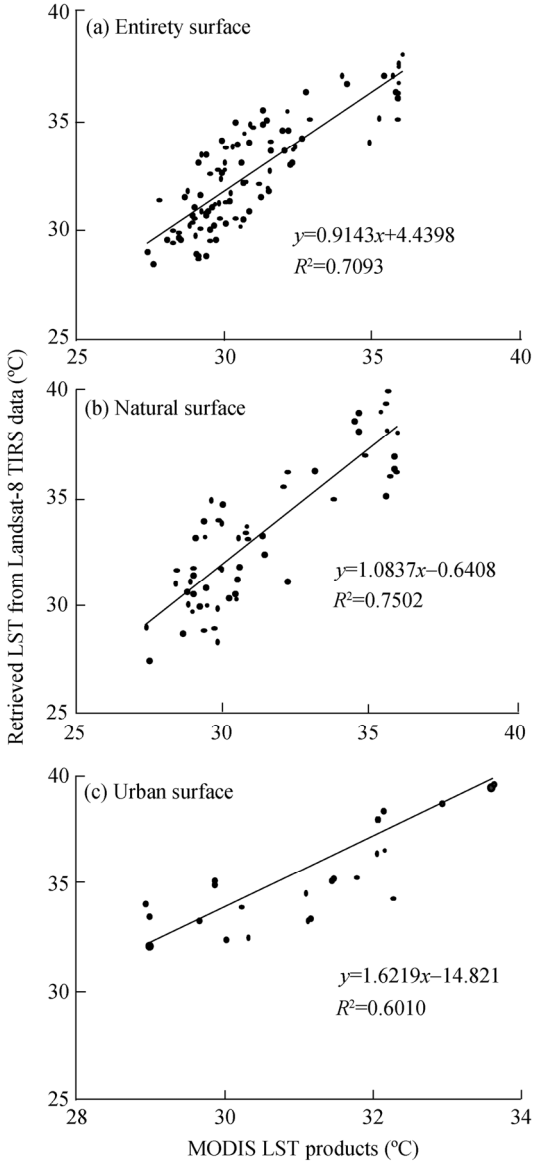

Fig. 7 Correlation analyses of retrieved LST from Landsat-8 TIRS data and MODIS LST products on entirety surface (a), natural surface (b) and urban surface (c)

Basing on the relevant analysis for the conjugate points (Fig. 7; Table 2), we found the correlation coefficients of retrieved LST from Landsat-8 TIRS and MODIS LST products on entirety surface, natural surface and urban surface were 0.8422, 0.8661 and 0.7345, respectively. Moreover, the sample points selected in the above two types both had passed T test using a significance level of 0.05, indicating that there is a strong correlation between the two variables.

Table 2 Correlation coefficients of retrieved LST from Landsat-8 TIRS and MODIS LST products on different land cover types

Land cover type	Correlation coefficient
Entirety surface	0.8422
Natural surface	0.8661
Urban surface	0.7345

Given that the retrieved LST is mixed with many non-urban pixels in the process of resampling the spatial resolution from 30 m to 1 km, the relative strong correlation coefficient shows that the retrieved result has certain reliability. In addition, we conducted a comparison of the sample points selected in the two images to calculate the mean and standard deviations of LST values for different land cover types (Fig. 8).

As can be seen from Fig. 8a, the value of retrieved LST from Landsat-8 is higher than that of MODIS LST products. There is a difference of 1.79°C between the entirety surface means while 1.98°C between the natural surface means. The closer standard deviations reflected that the two results are consistent in LST changes (Fig. 8b). There is a difference of approximately 4.63°C for the mean values of urban surface temperature (Fig. 8a), and the standard deviation difference is significant (Fig. 8b), indicating there are large changes in the retrieved LST value of TIRS. The experimental results may be due to the following reasons: (1) Intervals of 30 minutes existed between the two sensors as well as rapid changes in LST of impervious surfaces caused by high reflectivity such as town. (2) The water vapor content parameter required for producing MODIS LST products was retrieved from water vapor absorption property difference between different channels, which has some variance in the water vapor content data obtained by interpolation of surface vapor pressure based on observed values of the weather stations in this study and empirical correlation. (3) When determining the ground emissivity, this study reassigned specific emissivity values after classification without taking into account of emissivity

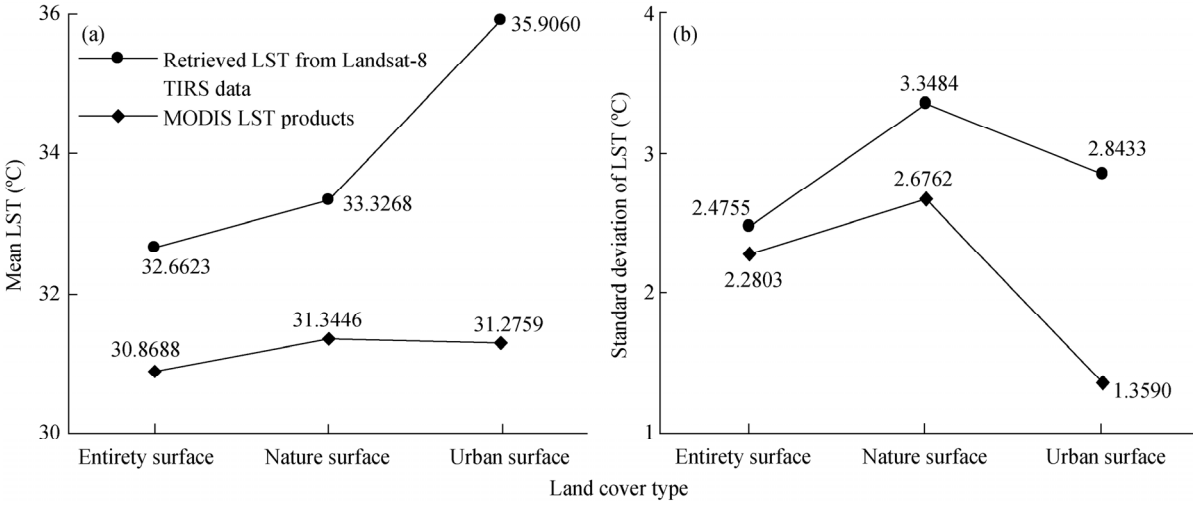

Fig. 8 Comparison of the LST between Landsat-8 TIRS and MODIS on different land cover types

difference in different channels. (4) In order to make a comparative analysis of the retrieved LST and MODIS LST products, we resampled the spatial resolution of retrieved LST from 30 m to 1 km, thus the spatial resolution difference resulted in a scale effect to some extent.

In summary, possible sources of errors have been identified and discussed. Nevertheless, under the specified constraints, retrieved LST conforms to the law of changes in natural LST, and a series of statistical indicators show that the results have a high reliability and accuracy.

3.2 Characteristics of LST

The land cover types in the study area include water body, town, bare land, grassland and arable land. Figure 9 shows the histogram distribution of LST in this area. During the acquisition of satellite imagery, LSTs were 30°C–40°C, and there were relative fewer areas with LST of higher than 40°C particularly in bare land.

LST was influenced by the combination of human activities and natural processes. In order to reveal the diversities of LST in different types of land cover, we analyzed the temperature characteristics of the three

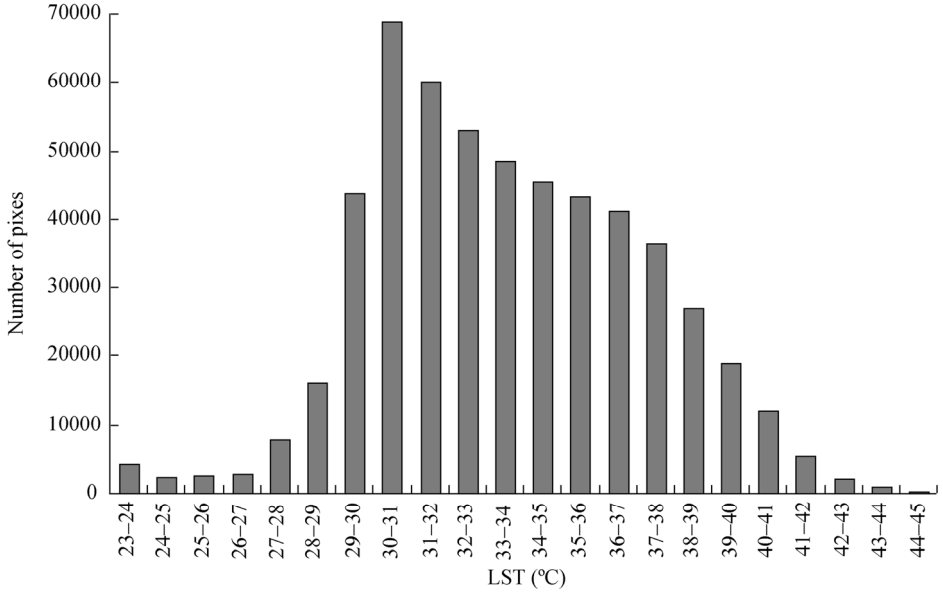

Fig. 9 Histogram distribution of LST in the study area

land cover types, including natural surface (composed of bare land, grassland and arable land), town (consist of road, industrial and mining district, city and rural residential area) and water body. The minimum, maximum and mean temperatures of the above three land cover patterns were derived by averaging all corresponding pixel values (Table 3). Table 3 showed that the average temperature of water body is the lowest one with the value of 29.42°C, while the average temperature of town is the highest, reaching 35.32°C.

Table 3 Difference of LST of different land cover types

Land cover type	LST		
	Minimum	Maximum	Mean
		(°C)	
Natural surface	24.58	46.12	33.03
Town	23.03	48.45	35.32
Water body	23.17	35.76	29.42

The preceding results reflect that the spatial variability of LST is basically consistent with the land cover types of the area. The hot spots clustered in high-density residential areas and heavy industrial districts, while the cold spots were mainly associated with lands adjacent to rivers, parks and farmlands. The main land cover type in the Tianshan mountainous area and the low-relief terrains in the mountain piedmont hilly area is sparse grassland with bush, and the low vegetation cover and high bareness lead to the high surface temperature. The Jiahezi Reservoir, located in the northeast corner of the area, is an evident low temperature region, because the reservoir water boasts so high thermal conductivity that it hardly aggregates heat. On the other hand, water may take away lots of heat through natural evaporation. Shihezi oasis is an arid agricultural irrigation area and the surface temperature of arable land covered by agricultural crop is relatively low. The agricultural crop may stop the rising of LST to prevent direct sunlight. Furthermore, lots of heat may be taken away by the agricultural crop through transpiration.

It should be worth noting that the areas with relatively high temperatures are centered in the northern urban area, where many industrial fields and residential areas with higher bareness degrees are distributed. Concrete buildings and surfaces could rapidly absorb solar radiation (Hall et al., 2012), resulting in extremely high temperatures. However, due to the increase in greening area, the LST in the central urban area is relatively low. Trees and vegetation brought lower surface and air temperatures by providing shade and through evapotranspiration, thus making afforestation a simple and effective way to reduce urban heat island effect.

4 Conclusions

Landsat-8 TIRS is one of the most accurate thermal infrared sensors with relatively high spatial resolutions at present. It has the capability to acquire information in two thermal infrared spectral bands of 10.90 and 12.0 μm. It may provide a better measurement of LST on the basis of split-window method. In this study, we put forward a modified algorithm for LST retrieval by using Landsat-8 TIRS data and meteorological observation. Firstly, we used the observed data of surface vapor pressure from AWS to estimate the parameters of atmospheric water vapor content, which were required for the calculation of atmospheric transmittance. Secondly, a classification map with high spatial resolution was used as a supplement to estimate ground emissivity. Finally, Qin's algorithm with improved higher precision in the split-window method was adopted for retrieving LST quantitatively from Landsat-8 TIRS data.

In addition, the MODIS LST products (MOD11A1) were used for validation and analysis of the retrieved LST. Analysis of correlation coefficients of retrieved LST from Landsat-8 TIRS data and MODIS LST products showed that the two kinds of LST have high consistency though the algorithms and data are different. The retrieved LST based on Landsat-8 TIRS data is in line with the law of changes in natural LST and is able to clearly reflect the spatial distribution of surface temperature in Shihezi. So the retrieved LST has a certain accuracy and reliability, and the modified algorithm used in this study is practical.

However, due to the lack of synchronous ground measured LST data during the satellite transit time, absolute accuracy assessment cannot be made on the retrieved LST. This study only made a preliminary

study from the perspective of quantitative application of Landsat-8 TIRS data. Further study and discussion is needed to achieve better application of Landsat-8 TIRS data into the fields, such as monitoring urban heat island and agricultural production.

Acknowledgements

This study was funded by the Project of Scientific and Technological Support to Xinjiang from Xinjiang Production and Construction Corps (2013AB017), the Doctorial Fund Project of Xinjiang Production and Construction Corps (2012BB001), the National Natural Science Foundation of China (31372354) and the International Science & Technology Cooperation Program of China (2013DFR30760).

References

Becker F, Li Z L. 1995. Surface temperature and emissivity at various scales: Definition, measurement and related problems. Remote Sensing Reviews, 12(3–4): 225–253.

Friedel M J. 2012. Data-driven modeling of surface temperature anomaly and solar activity trends. Environmental Modelling & Software, 37: 217–232.

Gao L, Qin Z H. 2007. Research on the fitting relation of the planck equation expansion parameter model in split window algorithm. Geography and Geo-Information Science, 23(4): 9–12.

Hall M R, Dehdezi P K, Dawson A R, et al. 2012 .Influence of the thermophysical properties of pavement materials on the evolution of temperature depth profiles in different climatic regions. Journal of Materials in Civil Engineering, 24(1): 32–47.

Irons J R, Dwyer J L, Barsi J A. 2012. The next Landsat satellite: The Landsat Data Continuity Mission. Remote Sensing of Environment, 122: 11–21.

Jiang L P, Qin Z H, Xie W. 2006. Retrieving atmospheric water vapor from modis near infrared data. Remote Sensing For Land & Resources, (3): 5–9, 88.

Jiménez-Muñoz J C, Sobrino J A. 2003. A generalized single-channel method for retrieving land surface temperature from remote sensing data. Journal of Geophysical Research: Atmospheres, 108(D22): 4688–4695.

Jiménez-Muñoz J C, Sobrino J A. 2010. A single-channel algorithm for land-surface temperature retrieval from ASTER data. Geoscience and Remote Sensing Letters, IEEE, 7(1): 176–179.

Katsiabani K, Adaktilou N, Cartalis C. 2009. A generalised methodology for estimating land surface temperature for non-urban areas of Greece through the combined use of NOAA–AVHRR data and ancillary information. Advances in Space Research, 43(6): 930–940.

Kaufman Y J, Gao B C. 1992. Remote sensing of water vapor in the near IR from EOS/MODIS. IEEE Transactions on Geoscience and Remote Sensing, 30(5): 871–884.

Li H, Liu Q H, Zhong B, et al. 2010. A single-channel algorithm for land surface temperature retrieval from HJ-1B/IRS data based on a parametric model. Geoscience and Remote Sensing Symposium (IGARSS), 2010 IEEE International, 2448–2451.

Li Z L, Tang B H, Wu H, et al. 2013. Satellite-derived land surface temperature: Current status and perspectives. Remote Sensing of Environment, 131(2013): 14–37.

Ma Y, Kuang Y Q, Huang N S. 2010. Coupling urbanization analyses for studying urban thermal environment and its interplay with biophysical parameters based on TM/ETM+ imagery. International Journal of Applied Earth Observation and Geoinformation, 12(2): 110–118.

Maimaitiyiming M, Ghulam A, Tiyip T, et al. 2014. Effects of green space spatial pattern on land surface temperature: Implications for sustainable urban planning and climate change adaptation. ISPRS Journal of Photogrammetry and Remote Sensing, 89: 59–66.

McMillin L M. 1975. Estimation of sea surface temperatures from two infrared window measurements with different absorption. Journal of Geophysical Research, 80(36): 5113–5117.

Peng S S, Piao S L, Zeng Z Z, et al. 2014. Afforestation in China cools local land surface temperature. Proceedings of the National Academy of Sciences, 111(8): 2915–2919.

Price J C. 1984. Land surface temperature measurements from the split window channels of the NOAA 7 Advanced Very High Resolution Radiometer. Journal of Geophysical Research: Atmospheres, 89(D5): 231–237.

Qin Z H, Olmo G D, Karnieli A. 2001a. Derivation of split window algorithm and its sensitivity analysis for retrieving land surface temperature from NOAA-advanced very high resolution radiometer data. Journal of Geophysical Research, 106(D19): 22655–22670.

Qin Z H, Karnieli A, Berliner P. 2001b. A mono-window algorithm for retrieving land surface temperature from Landsat TM data and its application to the Israel-Egypt border region. International Journal of Remote Sensing, 22(18): 3719–3746.

Qin Z H, Zhang M H, Arnon K. 2001c. Split window algorithms for retrieving land surface temperature from NOAA-AVHRR data. Remote Sensing For Land & Resources, 56(2): 33–42.

Sobrino J, Raissouni N, Li Z L. 2001. A comparative study of land surface emissivity retrieval from NOAA data. Remote Sensing of Environment, 75(2): 256–266.

Son N T, Chen C F, Chen C R, et al. 2012. Monitoring agricultural drought in the Lower Mekong Basin using MODIS NDVI and land surface temperature data. International Journal of Applied Earth Observation and Geoinformation, 18: 417–427.

Srivastava P K, Majumdar T J, Bhattacharya A K. 2009. Surface temperature estimation in Singhbhum Shear Zone of India using Landsat-7 ETM+ thermal infrared data. Advances in Space Research, 43(10): 1563–1574.

Stathopoulou M, Cartalis C, Petrakis M. 2007. Integrating Corine Land Cover data and Landsat TM for surface emissivity definition: application to the urban area of Athens, Greece. International Journal of Remote Sensing, 28(15): 3291–3304.

Van de Griend A A, Owe M. 1993. On the relationship between thermal emissivity and the normalized difference vegetation index for natural surfaces. International Journal of Remote Sensing, 14(6): 1119–1131.

Vinnikov K Y, Yu Y Y, Goldberg M D, et al. 2011. Scales of temporal and spatial variability of midlatitude land surface temperature. Journal of Geophysical Research: Atmospheres (1984–2012), 116(D2): 2156–2202.

Wan Z, Zhang Y, Zhang Q, et al. 2004. Quality assessment and validation of the MODIS global land surface temperature. International Journal of Remote Sensing, 25(1): 261–274.

Wan Z M. 2008. New refinements and validation of the MODIS land-surface temperature/emissivity products. Remote Sensing of Environment, 112(1): 59–74.

Yao J Q. 2012. Temporal-spatial distribution of the water vapor content and evolution character of water vapor during heavy rain in Tianshan Mountains. MSc Thesis. Urumqi: Xinjiang Normal University.

Zheng G Q, Lu M, Zhang T, et al. 2010. The impact of difference of land surface emissivity on the land surface temperature retrieval in Jinan City. Journal of Shandong Jianzhu University, 25(5): 519–523.

Zhou J, Zhan W F, Hu D Y, et al. 2010. Improvement of mono-window algorithm for retrieving land surface temperature from HJ-1B satellite data. Chinese Geographical Science, 20(2): 123–131.